

Benzotriazole-Containing D- π -A Conjugated Organic Dyes for Dye-Sensitized Solar Cells

Yung-Sheng Yen,^[a, b] Chang-Tze Lee,^[c] Chih-Yu Hsu,^[a] Hsien-Hsin Chou,^[a]
Yung-Chung Chen,^[a] and Jiann T. Lin*^[a, c]

Abstract: A series of metal-free benzotriazole-based dipolar dyes have been developed as sensitizers for dye-sensitized solar cells (DSSCs). Different heteroaromatic rings such as furan, thiophene, and selenophene, were used in combination with benzotriazole as the conjugated spacer group. Light har-

vesting, charge recombination, and electron injection of the cells fabricated are affected by the heteroaromatic ring

used in the spacer. The DSSC with the thiophene-containing dye has the highest conversion efficiency of 6.20%, which reaches 85% of the standard cell based on N719.

Keywords: benzotriazole • charge recombination • heterocycles • solar cells • sensitizers

Introduction

Dye-sensitized solar cells (DSSCs) have attracted considerable attention owing to their high incident solar-light-to-electricity conversion efficiency and low cost of production since the innovative report by Grätzel and O'Reagan in 1991.^[1] Currently, DSSCs sensitized by polypyridyl Ru^{II} complexes have achieved remarkably high conversion efficiencies that exceed 11% under air mass (AM 1.5G) illumination.^[2] More recently, porphyrin-based DSSCs have made a breakthrough and achieved an efficiency of 12.3%, which even surpasses that of ruthenium-based dyes for DSSCs.^[3] Although the ruthenium complexes showed high efficiency and long-term stability, they are quite expensive and hard to purify. Besides, the metal-to-ligand charge-transfer (MLCT) band in ruthenium dyes seldom exceeds 25 000 M⁻¹ cm⁻¹. In comparison, porphyrin compounds normally have only weak or negligible absorption in the wavelength region between the Soret and Q bands. Considerable research efforts have also been focused on the development of new metal-free organic dye sensitizers^[4] and a record high efficiency of 10.3% has been achieved.^[5] The intense absorption of metal-free

dyes is advantageous in solid-state DSSCs because a thinner TiO₂ film can be used to facilitate electron transport. This characteristic also allows metal-free dyes to complement the deficit in the absorption of ruthenium dyes for using in co-sensitized DSSCs with improved performance.^[6]

Organic sensitizers normally have a D- π -A dipolar architecture, which has a π -electron-rich moiety as the donor (D), a π -electron-deficient moiety as the acceptor (A), and a π -conjugated spacer as the bridge between the donor and the acceptor. Previously, we developed metal-free sensitizers with an electron-deficient benzothiadiazole (BT) unit in the conjugated spacer,^[7] and found that the BT unit effectively shifted the electronic absorption band to a longer wavelength. The best photon-to-electricity conversion efficiency of the DSSCs only reached approximately 70% of the standard cell based on *cis*-[Ru(NCS)₂(dcbpy)₂] (dcbpy = 2,2'-bipyridyl-4,4'-dicarboxylate) owing to partial charge trapping of the BT unit. Although we^[8a] and other research groups^[8b-f] found that significantly improved efficiencies could be achieved with BT-based sensitizers after appropriate modification of the conjugated spacer, partial charge trapping still remained.

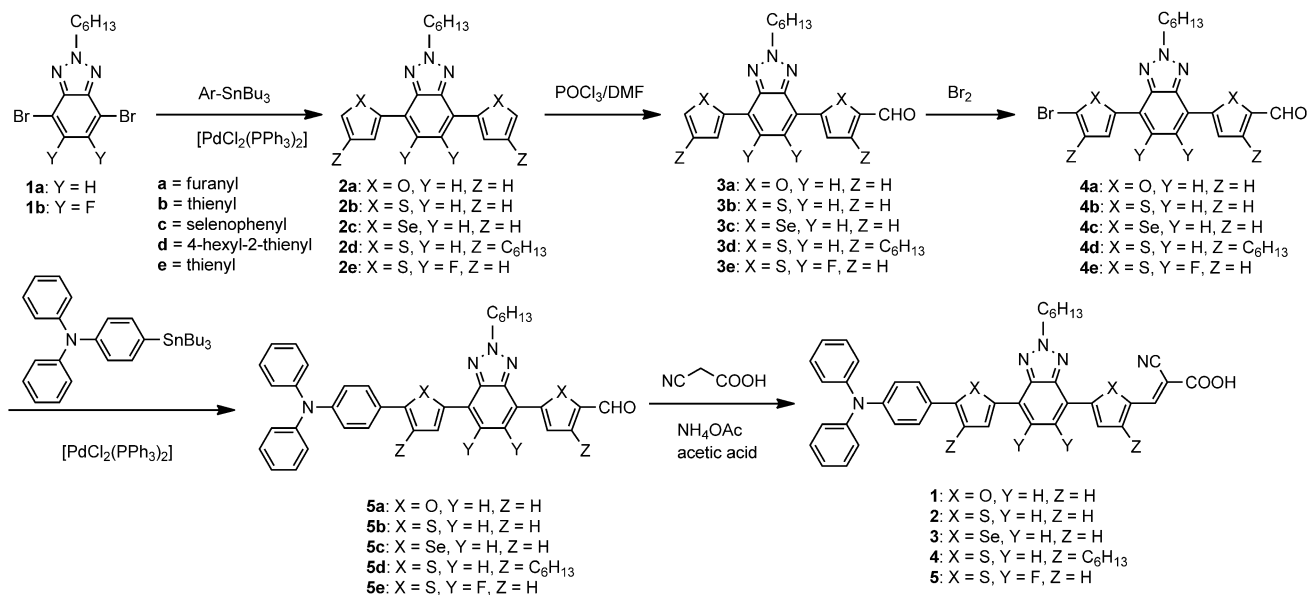
Benzotriazole (BTA), in which the sulfur atom of the benzothiadiazole is replaced by NR (R = alkyl group), is considered as a moderate electron-deficient heterocycle^[9] and has been widely used as the acceptor of semiconducting polymers for bulk heterojunction solar cells.^[10] However, unlike BT, the BTA unit has a higher lowest unoccupied molecular orbital (LUMO) energy level than the benzothiadiazole unit because of the higher basicity of the nitrogen atom than the sulfur atom.^[10b] With our continuing interest in metal-free sensitizers for DSSC applications, we therefore decided to incorporate the BTA moiety in the conjugated spacer of the dye because the charge trapping effect found in the BT congener might be alleviated. Though a slight blue shift in the absorption spectra is expected for the BTA compound com-

[a] Dr. Y.-S. Yen, Dr. C.-Y. Hsu, Dr. H.-H. Chou, Dr. Y.-C. Chen, Prof. Dr. J. T. Lin
Institute of Chemistry
Academia Sinica
Taipei, 115 (Taiwan)
E-mail: jtlin@gate.sinica.edu.tw

[b] Dr. Y.-S. Yen
Assistant Research Scholar of the National
Science Council of ROC

[c] C.-T. Lee, Prof. Dr. J. T. Lin
Department of Chemistry
National Central University
Chungli, 320 (Taiwan)

Supporting information for this article is available on the WWW under <http://dx.doi.org/10.1002/asia.201201173>.



Scheme 1. Synthesis of dyes **1–5**. DMF = *N,N*-dimethylformamide.

pared to the **BT** congener, incorporation of an alkyl chain at the 2-position of the **BTA** unit might not only improve the solubility of the dye, but also help to suppress the dark current by blocking the electrolytes from close contact with the TiO₂ surface. Herein, we report a new series of dyes with a benzotriazole entity in the conjugated spacer. DSSCs using these dyes as the sensitizers will be also discussed. Two papers were published while this research was still ongoing.^[11]

Results and Discussion

Synthesis of the Materials

The benzotriazole-based organic dyes (**1–5**) were synthesized as illustrated in Scheme 1. A Stille coupling reaction^[12] between 4,7-dibromo-2-hexylbenzotriazole and appropriate stannyl compounds provided substrates **2a–e**, which underwent subsequent formylation by Vilsmeier reaction to afford **3a–e**. Intermediates **5a–e** were obtained from a Stille coupling reaction of **3a–e** with tributylstannyl derivatives. Finally, a classical Knoevenagel reaction between 2-cyanoacetic acid and **5a–e** in acetic acid led to the desired products. These new dyes were fully characterized with ¹H NMR, ¹³C NMR spectroscopy, and HRMS.

Optical Properties

The absorption spectra of the dyes in a solution of THF are displayed in Figure 1, and the corresponding data are presented in Table 1. All the dyes have

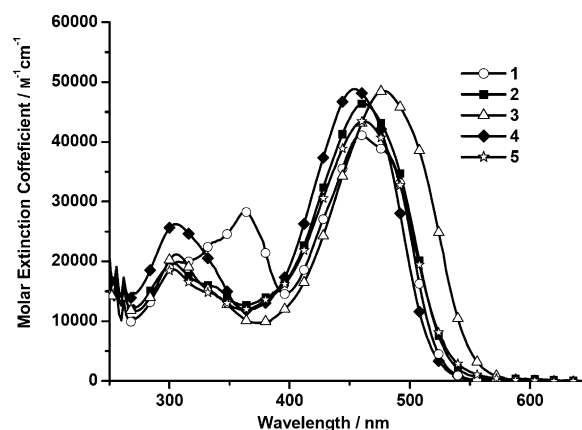


Figure 1. The absorption spectra of the dyes in THF.

a very intense absorption band around 454–478 nm (molar extinction coefficient (ϵ) = 4.10 – $4.88 \times 10^4 \text{ M}^{-1} \text{ cm}^{-1}$) attributable to the π - π^* transition with charge-transfer character (from the arylamine donor to the 2-cyanoacrylic acid acceptor). The maximum absorption wavelength of **1–3** (**1**: 460 nm; **2**: 462 nm; **3**: 478 nm) and the molar extinction coefficient (**1**: $4.10 \times 10^4 \text{ M}^{-1} \text{ cm}^{-1}$; **2**: $4.64 \times 10^4 \text{ M}^{-1} \text{ cm}^{-1}$; **3**:

Table 1. Electrooptical parameters of the dyes.

Dye	λ_{abs} ($\epsilon \times 10^{-4} [\text{M}^{-1} \text{ cm}^{-1}]$) ^[a] [nm]	λ_{em} ^[a] [nm]	$E_{1/2}(\text{ox})$ ^[b] [mV]	E_{ox} ^[c] [V]	E_{0-0} ^[c] [eV]	E_{0-0}^* ^[d] [V]
1	460 (4.10), 362 (2.83), 306 (2.01)	565	390 (101)	1.09	2.42	-1.23
2	462 (4.64), 304 (1.97)	583	459 (107)	1.16	2.39	-1.13
3	478 (4.85), 306 (2.12)	593	423 (165)	1.12	2.32	-1.10
4	454 (4.88), 306 (2.62)	580	513 (112)	1.21	2.43	-1.12
5	462 (4.35), 302 (1.87)	584	461 (109)	1.16	2.36	-1.10

[a] The absorption spectra were recorded in THF. [b] The cyclic voltammetric studies were conducted in CH₂Cl₂. Scan rate: 100 mV sec⁻¹, Electrolyte: (*n*-C₄H₉)₄NPF₆; ΔE_p is the separation between the anodic and cathodic peaks in units of mV. Potentials are quoted with reference to the internal ferrocene standard ($E_{1/2} = +265 \text{ mV vs Ag/AgNO}_3$). [c] E_{0-0} was determined from intersection of absorption and emission spectra in THF. [d] E_{0-0}^* : The excited state oxidation potential vs NHE.

$4.85 \times 10^4 \text{ M}^{-1} \text{ cm}^{-1}$) increased in the order of $1 < 2 < 3$. These observations are consistent with the electronegative effect reported by Wang et al. on metal-free dyes and Ru complexes that contain similar five-membered heteroaromatic units,^[13] that is, more electronegative atoms ($\text{O} > \text{S} > \text{Se}$) in the five-membered heteroaromatic units will result in a blue shift of the absorption band and a decreased molar extinction coefficient. The band at approximately 300 nm is attributed to the localized π - π^* transitions. An extra band at 362 nm for **1** could also be due to localized π - π^* transitions. The aggregation of the dye can be ruled out because the absorption profile is unaffected at lower dye concentrations.

The absorption band of **4** exhibited a hypsochromic shift compared with that of **2**, most likely the hexyl group tethered at the thiophene ring of **4** rendered the conjugated spacer less planar (see below) and deteriorated the electronic communication between the donor and the acceptor. The absorption wavelength of compound **2** is shorter (ca. 71 nm) than its congener^[8d] in which the benzotriazole entity is replaced with a benzothiadiazole entity, thereby indicating that the more electron-deficient benzothiadiazole unit can more effectively red shift the absorption. However, a higher tendency of charge trapping and dye aggregation in benzothiadiazole dyes could jeopardize the charge transfer and consequently electron injection from the excited dye molecule into the TiO_2 conduction band. Considering that incorporation of two electron-withdrawing fluorine groups at the 5- and 6-positions of the 2-(2-butyloctyl)-2*H*-benzo[*d*]-[1,2,3]triazole unit in a conjugated polymer results in a profound effect in the hole mobility of the polymer and thus the photovoltaic performance,^[10b] we also synthesized **5** for comparison. The absorption spectra of **2** and **5** are nearly superimposable, thus indicating that fluorine atoms have a negligible electronic effect on the 2-(2-butyloctyl)-2*H*-benzo[*d*]-[1,2,3]triazole unit.

The absorption spectra of the dyes adsorbed onto the TiO_2 film are shown in Figure 2. A blue shift in the absorption spectra relative to that in the solution might be caused by deprotonation of the carboxylic acid group.^[14] The spectra are also broadened at the long-wavelength side; this indicates possible existence of J-aggregation of the dyes. Com-

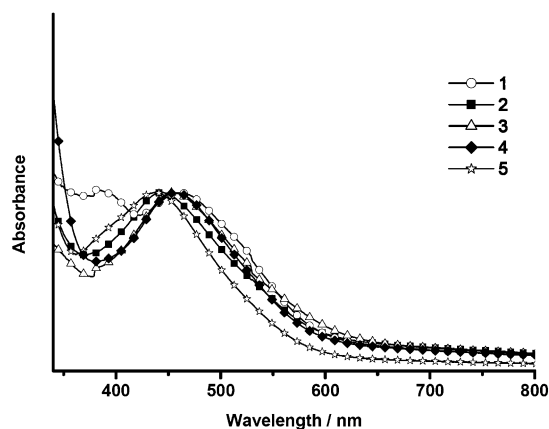


Figure 2. The absorption spectra of the dyes on TiO_2 .

pounds **1** and **4** have less blue shifts in the absorption, this might be because there is higher degree of aggregation upon dye adsorption. A somewhat higher degree of J-aggregation compared with other benzotriazole dyes^[11] might stem from the more planar structure of the dyes in this study. The aggregation was alleviated after addition of chenodeoxycholic acids (CDCA) as the co-adsorbent (Figure S1, see the Supporting Information). All the compounds are weakly emissive (Figure S2, see the Supporting Information), and the large Stokes shift ($>4000 \text{ cm}^{-1}$) is consistent with the charge-transfer nature of the emission (see below).

Electrochemical Properties

The highest occupied molecule orbital (HOMO) and LUMO of the dyes should match the potential of the conduction band edge of TiO_2 and the electrolyte redox potential, respectively, for facile electron injection and dye regeneration. Therefore, the electrochemical properties of the dyes were investigated. The electrochemical data of the compounds are listed in Table 1, and the representative cyclic voltammograms are shown in Figure 3. The first

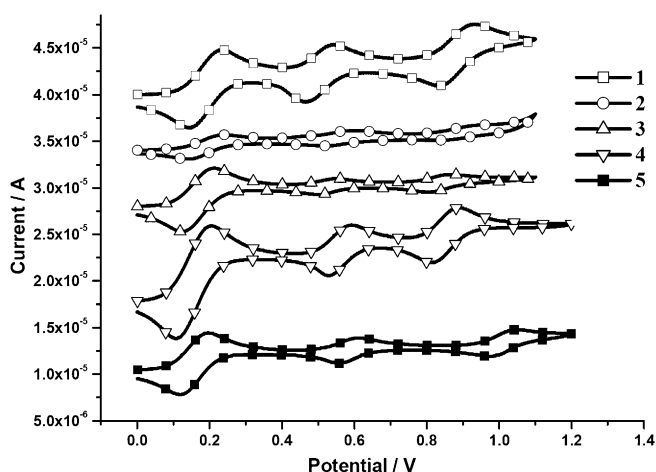


Figure 3. Cyclic voltammograms of **1-5** in deoxygenated CH_2Cl_2 containing 0.1 M TBAPF₆ at 25 °C. Ferrocene (Fc) was added as an internal standard. All potentials are in volts vs Ag/AgNO_3 (0.01 M in MeCN; the scan rate is 100 mVs^{-1}).

quasi-reversible one-electron redox wave can be attributed to the oxidation of the arylamine. Another quasi-reversible redox wave at a higher potential can be ascribed to the oxidation of the conjugated spacer. The excited state potential (E_{0-0}^*) of the sensitizer was estimated from the first oxidation potential (E_{ox}) at the ground state and the zero-zero excitation energy (E_{0-0}) estimated from the intersection of the absorption and the emission spectra. The E_{0-0}^* values (-1.10 to -1.23 V vs normal hydrogen electrode (NHE), see Table 1) deduced are more negative than the conduction-band-edge energy level of the TiO_2 electrode (-0.5 V vs NHE)^[15] and the first oxidation potentials of the dyes (1.09 to 1.21 V vs NHE) are more positive than the I^-/I_3^-

redox couple (ca. 0.4 V vs NHE).^[16] These results assure favorable electron injection and regeneration of the dye after electron injection.

Photovoltaic Devices

DSSCs were fabricated using these dyes as the sensitizers, with an effective area of 0.25 cm², nanocrystalline anatase TiO₂ particles, and the electrolyte composed of 0.05 M I₂/0.5 M LiI/0.5 M *tert*-butylpyridine in an acetonitrile solution. The performance parameters of the DSSCs fabricated using these dyes as the sensitizers under AM 1.5G illumination are listed in Table 2. The photocurrent–voltage (*J*–*V*) curves

Table 2. Performance parameters of DSSCs constructed using the dyes.

Dye	<i>J</i> _{sc} [mA cm ⁻²]	<i>V</i> _{oc} [V]	<i>FF</i>	<i>η</i> [%]
1	10.30	0.68	0.62	4.37
2	14.60	0.65	0.66	6.20
3	14.10	0.60	0.67	5.66
4	13.10	0.69	0.65	5.89
5	13.20	0.68	0.67	6.01
N719	15.10	0.74	0.66	7.33

and the incident photon-to-current conversion efficiencies (IPCEs) of the cells are shown in Figure 4 and 5, respectively. *J*-aggregation of the dyes (see above) is evident from the

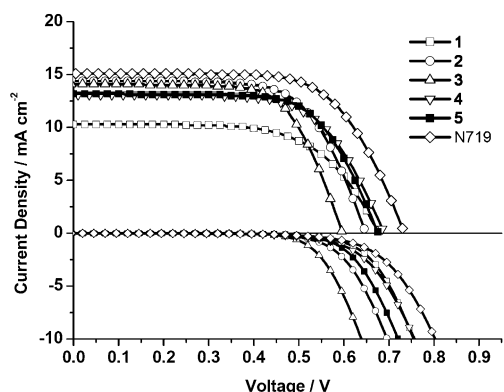


Figure 4. *J*–*V* curves and dark currents of DSSCs based on the dyes.

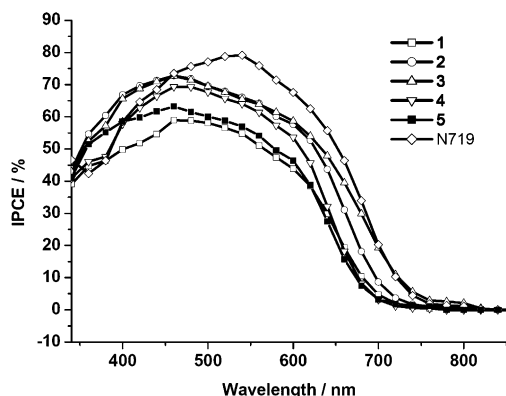


Figure 5. IPCE plots of the DSSCs using the dyes and N719.

broadened IPCE spectra compared to the absorption spectra of the dyes in the solution (Figure 1). Depending on the dyes, *J*-aggregation may improve the cell performance due to better light harvesting,^[17] or jeopardize the cell performance due to quenching of the excited dye molecules.^[18] In our case, the IPCE spectra have significant contribution from absorption at $\lambda_{\text{abs}} > 550$ nm. The DSSC based on **3** has IPCE spectra covering the same wavelength range as that of N719, which is consistent with the longest absorption wavelength of **3**. Because of the intense absorption of the dyes, the DSSCs of **2** and **3** have IPCE values surpassing those of N719 at wavelengths below 460 nm, and the DSSC of **4** has IPCE values comparable with those of N719 at wavelengths below 450 nm. However, the IPCE values of the DSSCs are significantly lower than those of N719 at longer wavelength. Consequently, the best conversion efficiency of the DSSCs in this study only reaches approximately 85% of the N719-based standard cell. The device efficiencies are in the order of **2** > **5** > **4** > **3** > **1**. The efficiency of the device based on **2** (6.20%) is significantly higher than that based on the benzo-thiadiazole congener ($\eta = 3.81\%$), which is only 42% of the N719-based standard cell ($\eta = 8.97\%$).^[8d]

Light absorption efficiency obviously plays an important role in cell performance. The DSSC based on **1** exhibited the lowest short-circuit current (*J*_{sc}), which is in conformity with its weaker charge-transfer absorption compared with the other dyes. Compared to the DSSC that is based on **2**, the significantly lower *J*_{sc} value of the DSSC based on **4** might be attributed to the shorter absorption and the lower adsorbed dye density of **4** than that of **2**. The adsorbed dye densities of the sensitizers on the TiO₂ surface were 3.69×10^{-7} , 3.29×10^{-7} , 4.19×10^{-7} , 1.83×10^{-7} , and 3.72×10^{-7} mol cm⁻² for **1**, **2**, **3**, **4**, and **5**, respectively. The lower dye density value of **4** than **2** might be due to the increased steric congestion imparted by **4** than **2** owing to the presence of two extra functional groups and less planar structure of **4**. DSSCs of **2** and **3** have larger *J*_{sc} values than the others; this could be ascribed to their intense charge-transfer bands. Compared with **2**, **5** has a lower *J*_{sc} value; this is likely owing to less-efficient light harvesting. In contrast, the open-circuit voltage (*V*_{oc}) value is higher in the cell of **5** owing to more effective suppression of the dark current (see below). The precise role of the fluorine substituents needs further investigation. The DSSC of **2** has a higher *V*_{oc} than that of its congener (0.54 V)^[8d] in which the benzotriazole entity is replaced with a benzothiadiazole entity. Similar to the observation of Wang et al.,^[19c] such a change could be relevant to the greater affinity of the more polarizable benzothiadiazole entity towards I₂ (or I₃⁻). The lower *V*_{oc} values for the DSSCs based on **2** and **3** could also be ascribed to the higher affinity of the sulfur and selenium atoms towards I₂ (or I₃⁻) in the two compounds, which increased the local concentration of iodine in the vicinity of the TiO₂ surface. A similar trend was found in furan- and thiophene-containing **BTA** dyes.^[12b] There have been many examples illustrating that dye molecules with polarizable sulfur-containing thiophene moieties have a stronger inter-

action with polarizable I_3^- and/or I_2 , thus leading to more facile charge recombination (dark current) and lower V_{OC} .^[19] A weak interaction between selenophene and I_2 may be an indication that tetrahydroselenophene is capable of forming a complex with molecular iodine.^[20] O'Regan pointed out that the I_2 binding with dyes results in facile charge recombination and lower V_{OC} .^[21] The binding coefficients for iodine and ruthenium dyes were measured by I_2 titration curves of dye-sensitized TiO_2 film. We also examined I_2 titration on dye-loaded TiO_2 films for probing the interaction between iodine and dyes **1** (furan), **2** (thiophene) and **3** (selenophene). The changes in the absorption spectra of the dyed films during I_2 titration are shown in Figure S3 (see the Supporting Information). Possibly due to weak interaction of the dyes with iodine, no obvious new peaks and isosbestic points were found in the titration spectra, thus preventing us from obtaining binding coefficients. Nonetheless, the decreased intensity of the absorbance spectra of the dye with a higher I_2 concentration in the order of decreasing rate (**3** > **2** > **1**) is consistent with the difference in V_{OC} . The similar trend in the V_{OC} found in furan and thiophene congeners reported by Hua et al.^[11b] could be due to the same reason.

As aforementioned, the extra functional groups in compound **4** affect the planarity of the conjugated spacer; this results in less dye adsorption as well as a blue shift in the absorption compared to **2**. It is worthy of note that the DSSC based on **4** has a higher V_{OC} and a smaller dark current (see below) than that of **2**. It is believed that extra functional groups help to decrease the void space among the dye molecules and block the close contact of the iodine molecules with the dyes. This also points out that other factors should not be overlooked, however, the interaction between iodine and heteroaromatic rings may play an important role.

Faster recombination of the electrons in the TiO_2 film with the oxidized electrolyte will lead to a larger dark current. The $J-V$ curves of the DSSCs under dark conditions are shown in Figure 4. The dark current value decreases in the order of **3** > **2** > **5** > **4** > **1**. The trend roughly conforms to that obtained from the electrochemical impedance studies. Electrochemical impedance spectroscopy (EIS) can provide important information on the interfacial charge recombination and redox reaction process in DSSCs. Figure 6 shows the Nyquist plots under a forward bias of -0.55 V in the dark. The middle-frequency regime is mainly related to the electron transport from the conduction band of TiO_2 to I_2 (or I_3^-) in the electrolyte. The charge recombination resistance (R_{rec}) at the TiO_2 surface can be deduced from the radius of the intermediate frequency by fitting curves using Z-view software.

The R_{rec} value increases in the order of **3** (85.42 Ω) < **2** (244.87 Ω) < **4** (385.80 Ω) < **5** (417.55 Ω) < **1** (545.43 Ω). As discussed earlier, the low affinity of the oxygen atom (in furan) towards I_2 (or I_3^-) can therefore more effectively suppress the charge recombination in the DSSC of **1**. In contrast, the high affinity of the selenium atom (in selenophene) towards I_2 (or I_3^-) results in a more facile charge recombination. The slight discrepancy between the EIS data

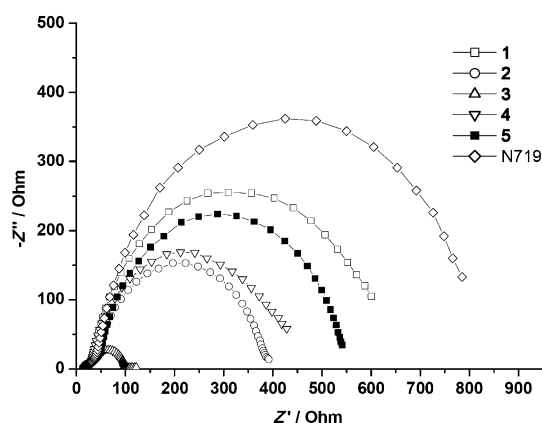


Figure 6. Nyquist plots of DSSCs in darkness.

and dark currents for DSSCs of **4** and **5** might be due to a different recombination rate of the electron with the oxidized dye, which is reflected in the EIS studies. The electron transport resistance (R_{tr}) of DSSCs can be deduced from the radius of the intermediate frequency semicircle in the Nyquist plots (Figure S4, see the Supporting Information) obtained from the electrochemical impedance measurement under illumination (100 mW cm^{-2} , open-circuit voltage conditions). The R_{tr} value decreases in the order of **1** (31.18 Ω) > **4** (17.31 Ω) > **3** (15.91 Ω) > **5** (15.33 Ω) > **2** (14.24 Ω). The lower electron transport resistance will assist electron collection and improve the cell efficiency. The much higher R_{tr} value for the DSSC based on **1** is in conformity with its lowest J_{SC} value. The difference in the R_{tr} value is small in DSSCs of other dyes.

Theoretical Approach

To correlate the molecular structures of the dyes with the performance of DSSCs, we carried out density functional theory (DFT) as well as time-dependent DFT (TDDFT) calculations at the B3LYP/6-31G* level of theory using a suite of Q-Chem 4.0 software. The results for the theoretical approach are summarized in Table S1 (see the Supporting Information). Compound **1** has a nearly planar structure in the optimized structure owing to the small amount of steric bulk imparted by the furan entity. In comparison, the dihedral angle between the phenyl ring of the triphenylamine and the larger thiophene or selenophene entity is larger than 20° (Figure 7), and the largest twist angle is found in **4**; this is due to the presence of the hexyl substituent in the thiophene ring. Selected frontier orbitals of the dyes are shown in Figure S5 (see the Supporting Information). The HOMO in these compounds is mainly distributed from the arylamine to the conjugated spacer, while the LUMO is largely distributed from 2-cyanoacrylic acid to the spacer. Figure 8 shows the detachment-attachment plots of dyes **1**, **2**, and **3** upon the $S_0 \rightarrow S_1$ transition, which features the points exactly where the hole densities (detachment) and the electron densities (attachment) reside. For all the compounds, the lowest energy transition ($S_0 \rightarrow S_1$) is nearly 100% of the HOMO \rightarrow

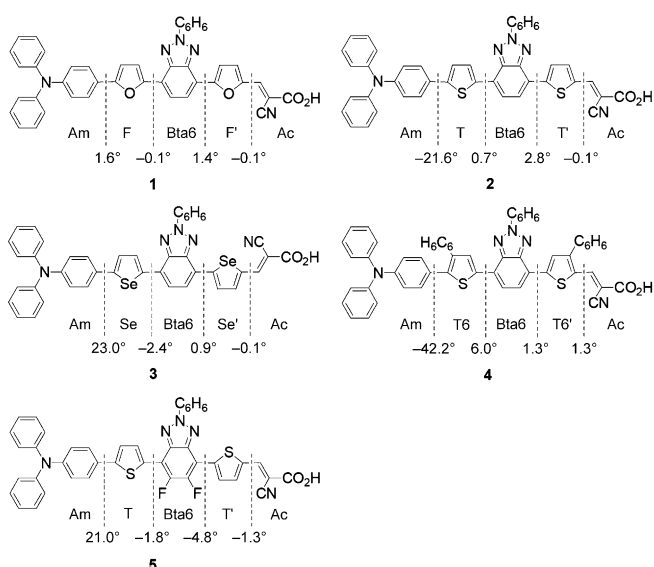


Figure 7. Schematic division and dihedral angles of molecules.

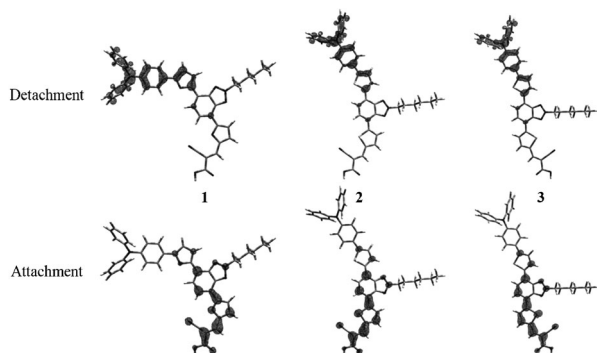


Figure 8. Calculated detachment-attachment plot of dyes 1, 2, and 3.

LUMO transition, thus confirming its charge-transfer character (arylamine to 2-cyanoacrylic acid). The high absorption intensity (calc. oscillator strength = 0.69–1.08) of the lowest energy band is attributed to the prominent contribution of the spacer to both the HOMO and LUMO. The Mulliken charges for the S_1 and S_2 states were calculated from the TDDFT results. Differences in the Mulliken charges in the excited and the ground states were calculated and grouped into several segments, triphenylamine (Am), heteroaromatic ring (F, T, Se, or T6), benzotriazole (Bta6, Bta6F), heteroaromatic ring (F', T', Se', or T6'), and 2-cyanoacrylic acid (Ac), to estimate the extent of charge separation upon excitation

(Table S1, see the Supporting Information). Figure 9 displays the changes in Mulliken charges of the dyes for the $S_0 \rightarrow S_1$ and $S_0 \rightarrow S_2$ transitions. Although there is negative charge at BTA, the Ac entity has an even higher negative charge. This is very different to those of BT dyes, in which the BT entity has a more negative Mulliken charge than the acceptor.^[7,8a] Clearly, a charge trapping effect is found in the BT dyes,^[7,8a] which is detrimental to electron injection is greatly alleviated in the BTA dyes.

Conclusions

New metal-free dyes comprising heteroaromatic ring, benzotriazole, and a heteroaromatic ring (furan, thiophene, or selenophene) as the conjugated spacer between the arylamine donor and 2-cyanoacrylic acceptor have been synthesized and used as the sensitizers for DSSCs. Compared to benzothiazole-containing congeners, there is less charge trapping in the benzotriazole unit, which is beneficial to electron injection. The heteroaromatic ring has great influence on the cell performance. The light-harvesting efficiency of the dyes decreases in the order of selenophene > thiophene > furan, and the efficiency of dark current suppression decreases in the order of furan > thiophene > selenophene. The thiophene-containing dye has the best cell performance, and the conversion efficiency reaches 6.20%, which is approximately 85% of the standard cell based on N719.

Experimental Section

General Information

Unless otherwise specified, all the reactions were performed under an atmosphere of nitrogen using standard Schlenk techniques. All solvents used were purified by standard procedures, or purged with nitrogen before use. ¹H NMR spectra were recorded on a Bruker 300 MHz or 400 MHz spectrometer. Absorption spectra were recorded on a Cary 50 probe UV/Vis spectrophotometer. All chromatographic separations were carried out on silica gel (60M, 230–400 mesh). Fast atom bombardment (FAB) mass spectra were recorded on a VG70-250S mass spectrometer.

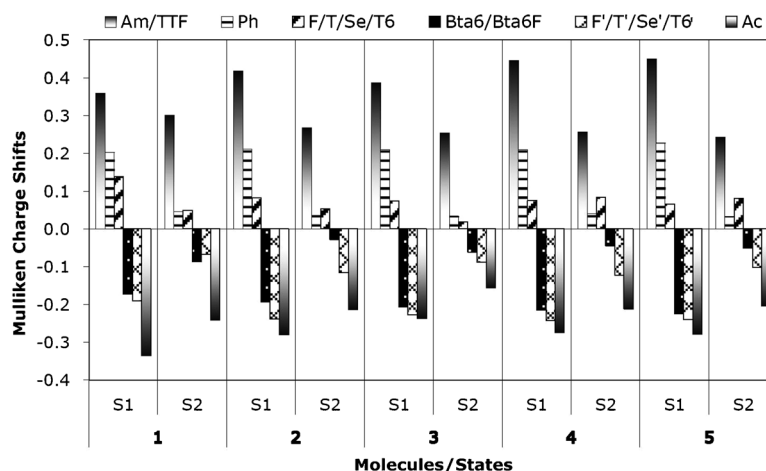


Figure 9. Plot of the difference in the Mulliken charges between the ground state and the excited state.

Elementary analyses were performed on a Perkin–Elmer 2400 CHN analyzer. The starting material 4,7-dibromo-2-hexyl-2H-benzotriazole was synthesized according to the literature method.^[22]

Assembly and characterization of DSSCs

The photoanode used was a TiO₂ thin film (12 μm of 20 nm particles as the absorbing layer and 6 μm of 400 nm particles as the scattering layer) coated on a fluorine-doped tin oxide (FTO) glass substrate^[23] with a dimension of 0.5 × 0.5 cm², and the film thickness was measured by a profilometer (Dektak3, Veeco/Sloan Instruments Inc., USA). A platinized FTO produced by thermopyrolysis of H₂PtCl₆ was used as a counter electrode. The TiO₂ thin film was dipped into the THF solution containing 3 × 10⁻⁴ M dye sensitizers for at least 12 h. After rinsing with THF, the photoanode adhered with a polyester tape of 30 μm in thickness and with a square aperture of 0.36 cm² was placed on top of the counter electrode and they were tightly clipped together to form a cell. The electrolyte was then injected into the space and the cell was sealed with the Torr Seal cement (Varian, MA, USA). The electrolyte was composed of 0.5 M lithium iodide (LiI), 0.05 M iodine (I₂), and 0.5 M 4-*tert*-butylpyridine that was dissolved in acetonitrile.

Iodine titration of dye-loaded TiO₂ films

The dye-loaded TiO₂ films on 1 mm glass substrates were placed in a one-sided 10 mm cuvette containing acetonitrile (2 mL). Upon the addition of a 0.01 M I₂ solution into the cuvette for the desired concentration, the measurement of the spectrum of the film and solution can be made, and subsequent rotation of the cuvette by 90 degrees allows measurement of the spectrum of the solution alone. The absorbance of the dye-loaded TiO₂ film alone was obtained by: $A_{\text{film}} = A_{\text{film+solution}} - 0.9A_{\text{solution}}$, where the factor 0.9 is due to the fraction of the thickness of the substrate (1 mm) based on the beam pathway (10 mm). For a more detailed method please refer to Ref. [21].

Quantum chemistry computation experiments

The computations were performed with Q-Chem 4.0 software.^[24] Geometry optimization of the molecules were performed using hybrid B3LYP functional and 6-31G* basis set. For each molecule, a number of possible conformations were examined and the one with the lowest energy was used. The same functional was also applied for the calculation of excited states using TDDFT. A number of previous studies exist that have employed TDDFT to characterize excited states with charge-transfer character.^[25] In some cases, an underestimation of the excitation energies was observed.^[25,26] Therefore, in the present study, we use TDDFT to visualize the extent of transition moments as well as their charge-transfer characters, and avoid drawing conclusions from the excitation energy.

The synthetic details for the intermediates of the desired products (1–5) are described in the Supporting Information.

General synthetic procedures for 1–5

Acetic acid (10 mL) was added to a flask containing a mixture of carbaldehyde precursor (1.0 mmol), cyanoacetic acid (1.3 mmol), and ammonium acetate (0.03 mmol). The mixture was heated at 100 °C for 8 h, and allowed to cool to room temperature. The resulting solid was filtered and washed with distilled water, diethyl ether, and methanol to give a dark red solid. Further purification by silica-gel chromatography using dichloromethane/acetic acid (50:1) as the eluent afforded the pure product.

2-Cyano-3-[5-[2-hexyl-7-(5-[4-[phenyl-(1-vinyl-propenyl)-amino]-phenyl]-furan-2-yl)]-2H-benzotriazol-4-yl]-furan-2-yl]-acrylic acid (1)

¹H NMR ([D₈]THF, 400 MHz): δ = 8.16 (d, *J* = 7.6 Hz, 1H), 8.02 (s, 1H), 8.10 (d, *J* = 3.6 Hz, 1H), 7.76 (d, *J* = 8.8 Hz, 2H), 7.69 (d, *J* = 3.6 Hz, 1H), 7.62 (d, *J* = 3.2 Hz, 1H), 7.46 (d, *J* = 3.2 Hz, 1H), 7.27 (t, *J* = 8.0 Hz, 4H), 1H), 7.09–7.12 (m, 6H), 7.02 (t, *J* = 7.2 Hz, 2H), 6.89 (d, *J* = 3.2 Hz, 1H), 4.87 (t, *J* = 7.2 Hz, 2H), 2.20 (m, 2H), 1.39 (m, 6H), 0.90 ppm (t, *J* = 7.2 Hz, 3H); ¹³C NMR ([D₈]THF, 100 MHz): δ = 164.3, 156.9, 155.9, 150.3, 149.5, 148.8, 148.7, 142.2, 141.5, 138.2, 130.3, 126.1, 125.6, 124.7, 124.3, 124.2, 122.7, 120.7, 117.8, 116.7, 115.9, 114.9, 107.9, 99.5, 57.7, 32.3, 31.0, 27.3, 23.5, 14.4 ppm; MS (FAB): *m/z*: 674.27 [*M*⁺]; elemental analy-

sis calcd (%) for C₄₂H₃₅N₅O₄: C 74.87, H 5.24, N 10.39; found: C 74.64, H 5.19, N, 10.44.

(Z)-2-Cyano-3-(5-(7-(5-(4-(diphenylamino)phenyl)thiophen-2-yl)-2-hexyl-2H-benzotriazol-4-yl)thiophen-2-yl)acrylic acid (2)

¹H NMR ([D₈]THF, 400 MHz): δ = 8.40 (s, 1H), 8.30 (d, *J* = 4.4 Hz, 1H), 8.10 (d, *J* = 4.0 Hz, 1H), 7.95 (d, *J* = 4.0 Hz, 1H), 7.91 (d, *J* = 7.6 Hz, 1H), 7.75 (d, *J* = 7.6 Hz, 1H), 7.62 (d, *J* = 8.4 Hz, 2H), 7.41 (d, *J* = 3.6 Hz, 1H), 7.27 (t, *J* = 8.8 Hz, 4H), 7.10 (t, *J* = 7.6 Hz, 4H), 7.05 (d, *J* = 6.0 Hz, 2H), 7.03 (d, *J* = 7.2 Hz, 2H), 4.90 (t, *J* = 7.2 Hz, 2H), 2.22 (m, 2H), 1.40 (m, 6H), 0.90 ppm (t, *J* = 7.2 Hz, 3H); ¹³C NMR ([D₈]THF, 100 MHz): δ = 163.1, 148.8, 147.7, 147.5, 145.4, 145.3, 141.9, 141.7, 138.4, 137.7, 135.7, 129.3, 129.2, 128.1, 127.6, 126.4, 125.7, 124.5, 124.3, 123.4, 123.1, 121.7, 121.4, 115.6, 99.1, 56.7, 31.2, 29.8, 26.2, 22.4, 13.3 ppm; MS (FAB): *m/z*: 706.23 [*M*⁺]; elemental analysis calcd (%) for C₃₄H₅₉N₅O₂S₂: C 74.19, H 6.80, N 8.01; found: C 73.96, H 6.75, N, 8.11.

2-Cyano-3-(5-[7-[5-(4-diphenylamino-phenyl)-selenophen-2-yl]-2-hexyl-2H-benzotriazol-4-yl]-selenophen-2-yl)-acrylic acid (3)

¹H NMR ([D₈]THF, 400 MHz): δ = 8.43 (s, 1H), 8.32 (d, *J* = 4.0 Hz, 1H), 8.29 (d, *J* = 4.0 Hz, 1H), 8.06 (d, *J* = 4.4 Hz, 1H), 7.92 (d, *J* = 7.6 Hz, 1H), 7.72 (d, *J* = 8.0 Hz, 1H), 7.56–7.54 (m, 2H), 7.26 (d, *J* = 8.0 Hz, 4H), 7.11 (d, *J* = 8.0 Hz, 4H), 7.05–7.01 (m, 4H), 4.90 (t, *J* = 7.2 Hz, 2H), 2.22 (m, 2H), 1.41 (m, 6H), 0.90 ppm (t, *J* = 7.2 Hz, 3H); ¹³C NMR ([D₈]THF, 100 MHz): δ = 164.3, 156.2, 153.3, 149.9, 148.9, 148.6, 143.7, 143.5, 143.0, 142.7, 142.4, 131.6, 131.5, 130.3, 129.0, 128.7, 127.8, 126.3, 125.6, 125.3, 124.7, 124.5, 124.2, 123.0, 117.4, 100.0, 57.8, 32.3, 30.9, 27.3, 23.5, 14.5 ppm; MS (FAB): *m/z*: 802.12 [*M*⁺]; elemental analysis calcd (%) for C₄₂H₃₅N₅O₂Se₂: C 63.08, H 4.41, N 8.76; found: C 63.22, H 4.61, N 8.55.

2-Cyano-3-(5-[7-[5-(4-diphenylamino-phenyl)-4-hexyl-thiophen-2-yl]-2-hexyl-2H-benzotriazol-4-yl]-3-hexyl-thiophen-2-yl)-acrylic acid (4)

¹H NMR ([D₈]THF, 400 MHz): δ = 8.52 (s, 1H), 8.15 (s, 1H), 8.02 (s, 1H), 7.80 (d, *J* = 7.6 Hz, 1H), 7.63 (d, *J* = 7.6 Hz, 1H), 7.39 (d, *J* = 8.4 Hz, 2H), 7.31 (t, *J* = 8.0 Hz, 4H), 7.18 (d, *J* = 7.6 Hz, 4H), 7.13 (d, *J* = 8.4 Hz, 2H), 7.08 (t, *J* = 7.6 Hz, 2H), 4.87 (t, *J* = 7.2 Hz, 2H), 2.93 (t, *J* = 7.6 Hz, 2H), 2.77 (t, *J* = 7.6 Hz, 2H), 2.25 (m, 2H), 1.75 (m, 4H), 1.52–1.36 (m, 18H), 1.33 ppm (t, *J* = 7.2, 9H); ¹³C NMR ([D₈]THF, 100 MHz): δ = 165.0, 156.3, 149.1, 149.0, 148.9, 144.3, 143.5, 143.2, 141.0, 140.7, 138.1, 132.0, 131.6, 131.1, 130.6, 129.7, 127.3, 126.1, 125.9, 124.6, 124.3, 123.0, 122.8, 117.3, 99.0, 58.0, 33.1, 33.0, 32.7, 32.6, 32.3, 31.2, 30.6, 30.4, 30.2, 30.1, 27.6, 24.0, 23.9, 23.8, 14.9, 14.89, 14.86 ppm; MS (FAB): *m/z*: 874.42 [*M*⁺]; elemental analysis calcd (%) for C₅₄H₅₉N₅O₂S₂: C 74.19, H 6.80, N 8.01; found: C 73.96, H 6.75, N, 8.11.

2-Cyano-3-(5-[7-[5-(4-diphenylamino-phenyl)-thiophen-2-yl]-5,6-difluoro-2H-benzotriazol-4-yl]-thiophen-2-yl)-acrylic acid (5)

¹H NMR ([D₈]THF, 400 MHz): δ = 8.45 (d, *J* = 4.4 Hz, 1H), 8.43 (s, 1H), 8.41 (d, *J* = 4.0 Hz, 1H), 8.04 (d, *J* = 3.6 Hz, 1H), 7.63 (d, *J* = 8.4 Hz, 2H), 7.45 (d, *J* = 2.4 Hz, 1H), 7.27 (t, *J* = 7.8 Hz, 4H), 7.13–7.02 (m, 8H), 4.89 (t, *J* = 7.4 Hz, 2H), 2.20 (m, 2H), 1.46–1.32 (m, 6H), 0.90 ppm (t, *J* = 7.2 Hz, 3H); ¹³C NMR ([D₈]THF, 100 MHz): δ = 164.1, 150.6, 149.3, 148.9, 148.8, 148.6, 146.4, 146.2, 141.7, 138.8, 138.6, 137.7, 133.6, 133.5, 131.8, 131.7, 131.2, 130.3, 128.8, 127.7, 125.7, 124.4, 123.8, 117.0, 102.0, 58.1, 32.3, 30.8, 27.3, 23.5, 14.5 ppm; MS (FAB): *m/z*: 741.20 [*M*⁺]; elemental analysis calcd (%) for C₄₂H₃₃F₂N₅O₂S₂: C 68.00, H 4.48, N 9.44; found: C 67.99, H 4.50, N, 9.52.

Acknowledgements

We acknowledge the support of the Academia Sinica (AC) and NSC (Taiwan) and the Instrumental Center of Institute of Chemistry (AC).

[1] M. Grätzel, B. O'Reagan, *Nature* **1991**, 353, 737–740.

- [2] a) Y. Chiba, A. Islam, Y. Watanabe, R. Komiya, N. Koide, L. Han, *Jpn. J. Appl. Phys.* **2006**, *45*, L638–L640; b) F. Gao, Y. Wang, D. Shi, J. Zhang, M. Wang, X. Jing, R. Humphry-Baker, P. Wang, S. M. Zakeeruddin, M. Grätzel, *J. Am. Chem. Soc.* **2008**, *130*, 10720–10728; c) C.-Y. Chen, M. Wang, J.-Y. Li, N. Pootrakulchote, L. Alibabaei, C.-h. Ngoc-le, J.-D. Decoppet, J.-H. Tsai, C. Grätzel, C.-G. Wu, S. M. Zakeeruddin, M. Grätzel, *ACS Nano* **2009**, *3*, 3103–3109; d) Y. Cao, Y. Bai, Q. Yu, Y. Cheng, S. Liu, D. Shi, F. Gao, P. Wang, *J. Phys. Chem. C* **2009**, *113*, 6290–6297; e) F. Sauvage, J.-D. Decoppet, M. Zhang, S. M. Zakeeruddin, P. Comte, M. Nazeeruddin, P. Wang, M. Grätzel, *J. Am. Chem. Soc.* **2011**, *133*, 9304–9309.
- [3] a) T. Bessho, S. M. Zakeeruddin, C.-Y. Yeh, E. W.-G. Diau, M. Grätzel, *Angew. Chem.* **2010**, *122*, 6796–6799; *Angew. Chem. Int. Ed.* **2010**, *49*, 6646–6649; b) A. Yella, H.-W. Lee, H. N. Tsao, C. Yi, A. K. Chandiran, M. K. Nazeeruddin, E. W.-G. Diau, C.-Y. Yeh, S. M. Zakeeruddin, M. Grätzel, *Science* **2011**, *334*, 629–634.
- [4] a) N. Robertson, *Angew. Chem.* **2006**, *118*, 2398–2405; *Angew. Chem. Int. Ed.* **2006**, *45*, 2338–2345; b) N. Robertson, *Angew. Chem.* **2008**, *120*, 1028–1030; *Angew. Chem. Int. Ed.* **2008**, *47*, 1012–1014; c) Z. Ning, H. Tian, *Chem. Commun.* **2009**, 5483–5495; d) Y. Ooyama, Y. Harima, *Eur. J. Org. Chem.* **2009**, 2903–2934; e) A. Mishra, M. K. R. Fischer, P. Bäuerle, *Angew. Chem.* **2009**, *121*, 2510–2536; *Angew. Chem. Int. Ed.* **2009**, *48*, 2474–2499; f) A. Hagfeldt, G. Boschloo, L. Sun, L. Kloo, H. Pettersson, *Chem. Rev.* **2010**, *110*, 6595–6663; g) Y.-S. Yen, H.-H. Chou, Y.-C. Chen, C.-Y. Hsu, J. T. Lin, *J. Mater. Chem.* **2012**, *22*, 8734–8747.
- [5] W. Zeng, Y. Cao, Y. Bai, Y. Wang, Y. Shi, M. Zhang, F. Wang, C. Pan, P. Wang, *Chem. Mater.* **2010**, *22*, 1915–1925.
- [6] a) K.-M. Lee, Y.-C. Hsu, M. Ikegami, T. Miyasaka, K. R. Justin Thomas, J. T. Lin, K.-C. Ho, *J. Power Sources* **2011**, *196*, 2416–2421; b) S.-Q. Fan, C. Kim, B. Fang, K.-X. Liao, G.-J. Yang, C.-J. Li, J.-J. Kim, J. Ko, *J. Phys. Chem. C* **2011**, *115*, 7747–7754; c) L. Han, A. Islam, H. Chen, C. Malapaka, B. Chiranjeevi, S. Zhang, X. Yang, M. Yanagida, *Energy Environ. Sci.* **2012**, *5*, 6057–6060.
- [7] M. Velusamy, K. R. Justin Thomas, J. T. Lin, Y.-C. Hsu, K.-C. Ho, *Org. Lett.* **2005**, *7*, 1899–1902.
- [8] a) H.-H. Chou, Y.-C. Chen, H.-J. Huang, T.-H. Lee, J. T. Lin, C. Tsai, K. Chen, *J. Mater. Chem.* **2012**, *22*, 10929–10938; b) J.-J. Kim, H. Choi, J.-W. Lee, M.-S. Kang, K. Song, S. O. Kang, J. Ko, *J. Mater. Chem.* **2008**, *18*, 5223–5229; c) Z.-M. Tang, T. Lei, K.-J. Jiang, Y.-L. Song, J. Pei, *Chem. Asian J.* **2010**, *5*, 1911–1917; d) W. Zhu, Y. Wu, S. Wang, W. Li, X. Li, J. Chen, Z.-s. Wang, H. Tian, *Adv. Funct. Mater.* **2011**, *21*, 756–763; e) D. H. Lee, M. J. Lee, H. M. Song, B. J. Song, K. D. Seo, M. Pastore, C. Anselmi, S. Fantacci, F. D. Angelis, M. K. Nazeeruddin, *Dyes Pigm.* **2011**, *91*, 192–198; f) S. Haid, M. Marszalek, A. Mishra, M. Wielopolski, J. Teuscher, J.-E. Moser, R. Humphry-Baker, S. M. Zakeeruddin, M. Grätzel, P. Bäuerle, *Adv. Funct. Mater.* **2012**, *22*, 1291–1302.
- [9] A. Tanimoto, T. Yamamoto, *Macromolecules* **2006**, *39*, 3546–3552.
- [10] a) L. Zhang, C. He, J. Chen, P. Yuan, L. Huang, C. Zhang, W. Cai, Z. Liu, Y. Cao, *Macromolecules* **2010**, *43*, 9771–9778; b) S. C. Price, A. C. Stuart, L. Yang, H. Zhou, W. You, *J. Am. Chem. Soc.* **2011**, *133*, 4625–4631.
- [11] a) Y. Cui, Y. Wu, X. Lu, X. Zhang, G. Zhou, F. B. Miapheh, W. Zhu, Z.-S. Wang, *Chem. Mater.* **2011**, *23*, 4394–4401; b) J. Mao, F. Guo, W. Ying, W. Wu, J. Li, J. Hua, *Chem. Asian J.* **2012**, *7*, 982–991.
- [12] J. K. Stille, *Angew. Chem.* **1986**, *98*, 504–519; *Angew. Chem. Int. Ed. Engl.* **1986**, *25*, 508–524.
- [13] a) R. Li, X. Lv, D. Shi, D. Zhou, Y. Cheng, G. Zhang, P. Wang, *J. Phys. Chem. C* **2009**, *113*, 7469–7479; b) F. Gao, Y. Cheng, Q. Yu, S. Liu, D. Shi, Y. Li, P. Wang, *Inorg. Chem.* **2009**, *48*, 2664–2669.
- [14] K. R. Justin Thomas, Y. C. Hsu, J. T. Lin, K. M. Lee, K. C. Ho, C. H. Lai, Y. M. Cheng, P. T. Chou, *Chem. Mater.* **2008**, *20*, 1830–1840.
- [15] J. He, W. Wu, J. Hua, Y. Jiang, S. Qu, J. Li, Y. Long, H. Tian, *J. Mater. Chem.* **2011**, *21*, 6054–6062.
- [16] A. Hagfeldt, M. Grätzel, *Chem. Rev.* **1995**, *95*, 49–68.
- [17] a) S.-L. Li, K.-J. Jiang, K.-F. Shao, L.-M. Yang, *Chem. Commun.* **2006**, 2792–2794; b) H.-Y. Yang, Y.-S. Yen, Y.-C. Hsu, H.-H. Chou, J. T. Lin, *Org. Lett.* **2010**, *12*, 16–19.
- [18] a) K. Hara, T. Sato, R. Katoh, A. Furube, Y. Ohga, A. Shinpo, S. Suga, K. Sayama, H. Sugihara, H. Arakawa, *J. Phys. Chem. B* **2003**, *107*, 597–606; b) K. Hara, Y. Tchibana, Y. Ohga, A. Shinpo, S. Suga, K. Sayama, H. Sugihara, H. Arakawa, *Sol. Energy Mater. Sol. Cells* **2003**, *77*, 89–103.
- [19] a) T. Marinado, K. Nonomura, J. Missfolk, M. K. Karlsson, D. P. Hadberg, L. Sun, S. Mori, A. Hagfeldt, *Langmuir* **2010**, *26*, 2592–2598; b) Z. Ning, Y. Fu, H. Tian, *Energy Environ. Sci.* **2010**, *3*, 1170–1181; c) M. Zhang, J. Liu, Y. Wang, D. Zhou, P. Wang, *Chem. Sci.* **2011**, *2*, 1401–1406; d) B. C. O'Regan, K. Walley, M. Juozapavicius, A. Anderson, F. Martar, T. Ghaddar, S. M. Zakeeruddin, C. Klein, J. R. Durrant, *J. Am. Chem. Soc.* **2009**, *131*, 3541–3548.
- [20] H. Hope, J. D. McCulloch, *Acta Crystallogr.* **1964**, *17*, 712–718.
- [21] X. Li, A. Reynal, P. Barnes, R. Humphry-Baker, S. M. Zakeeruddin, F. De Angelis, B. C. O'Regan, *Phys. Chem. Chem. Phys.* **2012**, *14*, 15421–15428.
- [22] Z. Zhang, P. Peng, P. Liu, C. Pan, Y. Li, Y. He, K. Zhou, Y.-P. Zhou, *Polym. Chem.* **2010**, *1*, 1441–1447.
- [23] Y.-S. Yen, Y.-C. Chen, Y. C. Hsu, H.-H. Chou, J. T. Lin, D.-J. Yin, *Chem. Eur. J.* **2011**, *17*, 6781–6788.
- [24] Q-CHEM, Version 4.0, Y. Shao, L. Fusti-Molnar, Y. Jung, J. Kussmann, C. Ochsenfeld, S. T. Brown, A. T. B. Gilbert, L. V. Slipchenko, S. V. Levchenko, D. P. O'Neill, R. A. DiStasio, Jr., R. C. Lochan, T. Wang, G. J. O. Beran, N. A. Besley, J. M. Herbert, C. Y. Lin, T. Van Voorhis, S. H. Chien, A. Sodt, R. P. Steele, V. A. Rassolov, P. E. Maslen, P. P. Korambath, R. D. Adamson, B. Austin, J. Baker, E. F. C. Byrd, H. Dachsel, R. J. Doerksen, A. Dreuw, B. D. Dunietz, A. D. Dutoi, T. R. Furlani, S. R. Gwaltney, A. Heyden, S. Hirata, C.-P. Hsu, G. Kedziora, R. Z. Khaliullin, P. Klunzinger, A. M. Lee, M. S. Lee, W. Liang, I. Lotan, N. Nair, B. Peters, E. I. Proynov, P. A. Pieniazek, Y. M. Rhee, J. Ritchie, E. Rosta, C. D. Sherrill, A. C. Simmonett, J. E. Subotnik, H. L. Woodcock III, W. Zhang, A. T. Bell, A. K. Chakraborty, D. M. Chipman, F. J. Keil, A. Warshel, W. J. Hehre, Z. Gan, Y. Zhao, N. E. Schultz, D. Truhlar, E. Epifanovsky, M. Oana, R. Baer, B. R. Brooks, D. Casanova, J.-D. Chai, C.-L. Cheng, C. Cramer, D. Crittenden, A. Ghysels, G. Hawkins, E. G. Hohenstein, C. Kelley, W. Kurlancheek, D. Liotard, E. Livshits, P. Manohar, A. Marenich, D. Neuhäuser, R. Olson, M. A. Rohrdanz, K. S. Thanthiriwatte, A. J. W. Thom, V. Vanovschi, C. F. Williams, Q. Wu, Z.-Q. You, E. Sundstrom, J. Parkhill, K. Lawler, D. Lambrecht, M. Goldey, R. Olivares-Amaya, Y. Bernard, L. Vogt, M. Watson, J. Liu, S. Yeganeh, B. Kaduk, O. Vydrov, X. Xu, C. Zhang, N. Russ, I. Y. Zhang, W. A. Goddard, III., N. Besley, A. Ghysels, A. Landau, M. Wormit, A. Dreuw, M. Diedenhofen, A. Klamt, A. W. Lange, D. Ghosh, D. Kosenkov, A. Landou, D. Zuev, J. Deng, S. P. Mao, Y. C. Su, D. Small, H. F. Schaefer, III., J. Kong, A. I. Krylov, P. M. W. Gill, M. Head-Gordon, Q-Chem, Inc., Pittsburgh, PA, **2008**.
- [25] a) H. M. Vaswani, C.-P. Hsu, M. Head-Gordon, G. R. Fleming, *J. Phys. Chem. B* **2003**, *107*, 7940–7946; b) Y. Kurashige, T. Nakajima, S. Kurashige, K. Hirao, Y. Nishikitani, *J. Phys. Chem. A* **2007**, *111*, 5544–5548.
- [26] A. Dreuw, M. Head-Gordon, *J. Am. Chem. Soc.* **2004**, *126*, 4007–4016.

Received: December 11, 2012
Published online: February 7, 2013